Master's thesis

NTNU
Norwegian University of Science and Technology
Faculty of Information Technology and Electrical Engineering
Department of Electronic Systems

Jostein Gjesdal

Polarization sensing in an urban environment

Exploring the sensing potential of telecom infrastructure

Master's thesis in MTELSYS
Supervisor: Dag Roar Hjelme
Co-supervisor: Steinar Bjørnstad
July 2023

NTNU
Norwegian University of
Science and Technology

Jostein Gjesdal

Polarization sensing in an urban environment

Exploring the sensing potential of telecom infrastructure

Master's thesis in MTELSYS
Supervisor: Dag Roar Hjelme
Co-supervisor: Steinar Bjørnstad
July 2023

Norwegian University of Science and Technology
Faculty of Information Technology and Electrical Engineering
Department of Electronic Systems

NTNU
Norwegian University of
Science and Technology

NTNU
Kunnskap for en bedre verden

Department of Electronic systems

Polarization sensing in an urban environment

Exploring the sensing potential in telecom infrastructure

Author:
Jostein Gjesdal
Supervisors:
Dag Roar Hjelme, Steinar Bjørnstad

Date: 7th July 2023

Table of Contents

List of Figures

List of Tables

Abstract

Optical fiber networks have become the primary information carrier in the global world. As the global network of fiber optic cables burgeons, it opens up possibilities for new complimentary applications of the fiber network, in addition to their primary data transfer functions. In this work we analyse the polarization of the light in a fiber optic telecommunications system, to use the fiber as a distributed sensor without disrupting the data flow. We utilized spectrographic techniques on data from an instrument deployed on a telecom system in Sarpsborg. We have been able to detect current surges in the power grid. The technique was also applied for traffic monitoring. Road traffic was monitored with limited results. Monitoring train traffic showed significant potential. We were also able to utilize the 50 Hz signal as a carrier signal to a limited degree. With further work we expect to be able to positively detect road traffic and other more specific activities near the fiber.

Chapter 1

Introduction

1.1 Why SOP sensing?

State of polarization or SOP sensing is a rapidly developing technology based on monitoring the state of polarization of light propagating in fiber optic telecom systems. The light in an optical fiber will vary its state of polarization in the presence of mechanical vibrations and strong electromagnetic fields. By continuously monitoring the SOP in the fiber it should be possible to detect signals from the environment along the fiber.

There are several advantages to developing this technology, the first and foremost is the low cost of implementation, as well as allowing us to leverage the already existing telecom infrastructure. SOP sensing utilizes the polarization information already in the signal, it only needs to be extracted. SOP sensing also has almost unlimited range along the fiber. The downside of SOP sensing is a lack of spatial resolution, it is impossible to detect where along the fiber a signal originated without several separated measurement cables. It can also be retrofitted on existing installations by addition of a simple and compact instrument.

There are alternatives to SOP based sensing, the most well established is distributed acoustic sensing (DAS). This is a more developed technology, however it is orders of magnitude more expensive to procure compared to SOP sensing. It also has a limited range of around 150 km in the best case. In return it has the advantage of having very high spatial resolution. Another alternative would be to phase based sensing. This technology is based on measuring phase changes of the light using an interferometric receiver. This requires using a ultra-narrow bandwidth laser common in metrology, these lasers and the interferometers needed to measure phase are neither cheap nor easy to work with. [1]

One of the major uses of the SOP technology is monitoring of the fiber cables themselves as well as other remote transmission infrastructure like power-lines and transportation pipelines. Infrastructure security is becoming an increasing concern for both corporations and national states. A recent report by the Norwegian national security [2] states that security on underseas infrastructure is lacking. This underseas infrastructure is critical. Effective monitoring and detection is the first line of defence of any security system. With underseas infrastructure spanning several 100km we are far outside the range of most sensor systems save deploying individual sensors along the fibers at vast cost. SOP sensing is one of the most cost effective ways to monitor remote infrastructure spanning oceans. Sub-sea deployment could also gives access to some of the most remote and under-sampled environments in the world for a wide range of science purposes from seismology to climate science. An additional advantage of proliferating the technology is that each additional sensing fiber can be used in fusion with existing fibers to increase the spatial resolution of the sensors exhibiting a strong network effect. The potential applications are not only limited to sub-sea monitoring, utilizing the technology on inland fiber infrastructure could allow detection of anomalous activity around the fibers that could help prevent service outages due to accidental damage from road works and similar activity.

1.2 Recent developments in the field of SOP sensing

SOP sensing is a small and new research field. While the physics behind polarization and its interaction with both acoustics and electromagnetics is well understood it is only with the recent expansion of global fiber optic networks that development of polarization for distributed sensing has taken on speed. Mecozzi et al showed how birefringence perturbations will translate to polarization perturbations from a theoretical perspective in [3]. The same team also used SOP monitoring for both seismological and oceanographic on a 10 500 km transoceanic cable along the west coast of the Americas they were able to detect both ocean swells and earthquakes along the same 10 500 km cable.

In [1] Cantano et al, also discusses future potential applications in early warnings systems for tsunamis and earthquakes. Thought there is significant work left particularly on the data management and processing side.

Detections of interference from strong electric fields have also been conducted in a controlled labratory setting. They detected huge polarization rotations in excess of 1 millon radians per second even when the simulated lightning strike only traveled along the fiber for a few meters.

Attempts to utilize SOP sensing for monitoring urban environments has been attempted before. In [4] A fiber was buried along a train track in the Czech republic, They were able to detect both temperature dependencies and the passing of trains on a bridge, as their cable was unburied and put in a cable box along the tracks on the bridge causing a spike in sensitivity at the bridge. The paper uses two polarimeters concurrently, both a Bragg grating based polarimeter capable of measuring all 4 Stokes parameters, as well as a polarizing beamsplitter similar to the one used in this work.

Another work in urban detection showed an ability to detect road traffic using again a polarizing beamsplitter. They were able to detect road traffic using a time domain approach. By looking for pairs of spikes originating from the axles of cars driving over high sensitivity spots. They were able to identify the signals as originating from cars and were even able to estimate the speed of the vehicle. [5]

1.3 Problem description

In this work we will process polarization data from an instrument already deployed on a telecom system to correlate patterns in the data and sources in the environment. The sensing system is designed to be an addition to the telecommunications system allowing us to utilize the already deployed fiber as a sensor with minimal cost and without disrupting the main data transfer function of the system. The cable lies in Sarpsborg, close to both a high-voltage power-line and road and rail traffic. This is an exploratory study, the goal is establishing the presence of information related to various activities, to . We will detect, characterize and identify the source of low frequency signals. Specifically focusing on road and rail traffic, and utilizing the 50 Hz signal.

- Is it possible to use the 50 Hz signals as a carrier wave?
- Is it possible to detect changes in power consumption on the power line?
- Is it possible to detect rush-hour traffic?
- Is it possible to detect train traffic?

Chapter 2

Theory

This chapter will first give an overview of the physical theory behind the sensors operating principles. First an introduction to light propagation in optical fibers will be given, we will then cover polarization and birefringence. We will also cover how polarization interacts with external electromagnetic and acoustic sources, and give an argument for why different mechanisms will interact to modulate each other. We will also cover the theory behind the signal processing used in our analysis.

2.1 Physics Foundation

In this section we will cover the physics behind SOP sensing. First we will cover wave propagation in fiber optics, then a brief introduction to polarization and birefringence before covering how birefringence perturbations manifest in fiber optics. We will also cover the most significant polarization altering interactions that give rise to the signals we see in our data.

2.1.1 Fiber Optic Wave Propagation

In order to understand the sensor principle used, an understanding of the propagation of light in fiber optics is required. As the key sensing mechanism is polarization, an electromagnetic optics approach is appropriate.

An optical fiber is a low-loss cylindrical dielectric waveguide, usually made of a glass like fused silica. The fiber consist of a core with refractive index n_1. The core is clad in another material with a lower refractive index $n_2 < n_1$. This structure is stretched out to form fibers only a few micrometers in diameter. Total internal reflection at the core-cladding boundary will guide the light through the fiber, keeping the energy contained and causing very low loss over large distances.[6]

There exist several types of fiber differentiated by their construction and propagation characteristics. The fiber used in our sensor is a single mode step index fiber. A single mode fiber is characterized by being so thin that only one mode of light propagation is supported in the fiber core at the frequency of the source in question. A step index fiber is a fiber where the boundary of the core and cladding is a discrete jump as contrasted by a graded index fiber where the refractive index follows a gradient from the core to the cladding.

The cross section of a step index fiber can be modeled as a homogeneous core with radius a surrounded by a cladding. Inside the core the refractive index is n_1, and in the cladding $n_2 < n_1$. The cylindrically symmetric refractive index is given by,

$$n(r) = \begin{cases} n_1 : r \leq a \\ n_2 : r > a \end{cases} \tag{2.1}$$

The **E** and **B** fields of a wave will follow the Helmholtz equation at all times.

$$\nabla^2 U + n^2(r) k_0 U = 0 \tag{2.2}$$

Where $k_0 = 2\pi/\lambda_0$, with λ_0 being the free-space wavelength of the light. Expressing the equation in cylindrical coordinates we have

$$\frac{\partial^2 U}{\partial r^2} + \frac{1}{r}\frac{\partial U}{\partial r} + \frac{1}{r^2}\frac{\partial^2 U}{\partial \phi^2} + \frac{\partial^2 U}{\partial z^2} + n^2(r) k_0 U = 0 \tag{2.3}$$

as the Helmholtz equation is a separable PDE, that is the solution can be written as $U(r, \phi, z) = R(r)\Phi(\phi)Z(z)$. We have cylindrical symmetry along the z-axis, thus the ϕ and z dependence are given by simple complex exponentials.

$$Z(z)` = e^{-j\beta z} \tag{2.4}$$

$$\Phi(\phi) = e^{-jl\phi} \tag{2.5}$$

The radial component is then given by one ODE for each region. By defining the parameters $k_T^2 = n_1^2 k_0^2 - \beta^2$ and $\gamma^2 = \beta^2 - n_2^2 k_0^2$. We can write

$$\frac{d^2 R}{dr} + \frac{1}{r}\frac{dR}{dr} + \left(k_T^2 - \frac{l^2}{r^2}\right) R = 0 \; for \, r < a \tag{2.6}$$

$$\frac{d^2 R}{dr} + \frac{1}{r}\frac{dR}{dr} - \left(\gamma^2 + \frac{l^2}{r^2}\right) R = 0 \; for \, r > a \tag{2.7}$$

The solutions of these differential equations known as the Bessel functions. In the core the solutions will be given by the l-th order Bessel functions of the first kind, $J_l(k_T r)$. In order to ensure that the Bessel functions are finite at the origin l must be a non-negative integer. These are also known as the cylindrical harmonics because they correspond to radial oscillations. In the cladding the solutions are the modified Bessel functions of the second kind of order l, $K_l(\gamma r)$. These functions are exponentially decaying functions. Again we require l to be an integer to ensure that the function is bounded.

The final cylindrical solutions are up to proportionality given by

$$U_l(r, \phi, z) \propto \begin{cases} J_l(K_T r) e^{-j(l\phi + \beta z)}, & r < a \\ K_l(\gamma r) e^{-j(l\phi + \beta z)}, & r > a \end{cases} \tag{2.8}$$

Both the E and B field of the guided wave must obey these equations, as well as the Maxwell equations and interface conditions. Denoting the core and cladding fields as $\mathbf{E}_{core}$ and $\mathbf{E}_{clad}$ and analogous for **H** fields, the additional equations that need to hold are as follows:

$$\mathbf{E}_{core}(a) = \mathbf{E}_{clad}(a) \tag{2.9}$$

$$\nabla \mathbf{E}_{core}(a) = \nabla \mathbf{E}_{clad}(a) \tag{2.10}$$

$$\mathbf{H}_{core}(a) = \mathbf{H}_{clad}(a) \tag{2.11}$$

$$\nabla \mathbf{H}_{core}(a) = \nabla \mathbf{H}_{clad}(a) \tag{2.12}$$

$$j\omega\epsilon_0 n^2 \mathbf{E} = \nabla \times \mathbf{H} \tag{2.13}$$

$$-j\omega\mu_0 \mathbf{H} = \nabla \times \mathbf{E} \tag{2.14}$$

$$\tag{2.15}$$

These equations apply in each direction independently. As there are no surface charges nor currents in the core cladding interface the interface conditions reduce to continuity conditions. We have approximated that the cladding is infinite, so we disregard the interface at the outside of the cladding.

We will also assume that the fiber is weakly guiding, that is $n_1 \approx n_2$ thus only approximately par-axial waves are guided. These additional constraints and the assumption of weak guidance reduce the boundary conditions to the requirement that the radial component, $R(r)$, is smooth at the interface for both fields. This gives approximately TEM waves. Having TEM waves is key for utilizing polarization as a sensing principle and allows us to use the standard representations of polarization as seen in the next section. [6]

Whether or not the fiber is single mode depends on how small the diameter of the core is and the propagation wavelength. The condition for a single mode fiber is

$$2\pi \frac{a}{\lambda_0} NA < 2.405 \tag{2.16}$$

where NA is the numerical aperture of the fiber. In a fiber satisfying this inequality only the fundamental LP_{01} mode will be supported. This also means there will only be one polarization state at any time instead of a super position of the polarization of all the modes. The indices 01 determine the mode number and the fields azimuthal distribution. [6]

2.1.2 Polarization

Polarization is the orientation of the Electromagnetic fields in a light wave. It is usually tracked by evaluating the orientation of the E-field in the x-y plane for a plane TEM wave traveling in the z-direction. The **E** field in the x direction, denoted $A_x = a_x e^{-i\phi_x}$ has an amplitude and a phase, the y-direction is analogous. The relation of these amplitudes and phases describe the polarization state.

The polarization of light can be characterized by the Stokes parameters. These are 4 parameters, S_0, S_1, S_2, S_3, defined as

$$S_0 = |A_x|^2 + |A_y|^2 \tag{2.17}$$
$$S_1 = |A_x|^2 - |A_y|^2 \tag{2.18}$$
$$S_2 = 2Re(A_x^* A_y) \tag{2.19}$$
$$S_3 = 2Im(A_x^* A_y) \tag{2.20}$$

The S_0 parameter represents the intensity of the light, usually we normalize with respect to this parameter. We can then represent the other three parameters on a unit sphere in 3D. S_1 determines the degree of polarization along the x and y axes, with $S_1 = 1$ representing fully x-polarized light and $S_1 = -1$ representing full polarization along the y-axis. $S_2 = 1$ corresponds to polarization along the 45° diagonal, $S_2 = -1$ along the 135° diagonal. $S_3 = 1$ is right hand circular polarization and -1 corresponds to left hand circular. These normalized parameters together form the Poincare sphere, a unit sphere fully describing any state of polarization(SOP)[6].

2.1.3 Birefringence

Birefringence is a phenomenon where the refractive index of a material is anisotropic, meaning it is not the same in every direction. This causes the propagation speed of light to be dependent on both polarization and propagation direction in the media.

in order to understand birefringence we consider the relation

$$\mathbf{E} = \epsilon^{-1}\mathbf{D} \tag{2.21}$$

In anisotropic materials ϵ^{-1} is a tensor defined as the inverse of the permeability ϵ. We define the impermeability tensor as $\eta = \epsilon_0\epsilon^{-1}$. In the principal axis coordinate system this tensor is by definition symmetric with $1/n_i$ on the main diagonal. Propagation where the electric field is along one of the principal axes are the normal modes of the material. A wave traveling along a principal axis with the electric field in the x direction will experience refractive index n_1, and like wise when the electric field points in the y direction it will experience refractive index n_2 and $E \parallel z$ experience $n = n_3$. These three modes can then be superpositioned to describe any wave in the medium, a super positioned wave will experience a polarization dependent effective refractive index, causing a difference in propagation speed. This difference in propagation speed will induce a polarization dependent phase shift given by:

$$\Delta\phi = \Delta nkL \tag{2.22}$$

where L is the length of the fiber, k is the wavenumber and Δn is the difference in effective refractive index between the polarization states. This phase shift changes the polarization state of the light. [6].

Fused silica is a glass, glasses are isotropic and thus not birefringent. There are several effects that can cause a normally isotropic material to exhibit birefringence like non-linear optical effects through the Pockels and Kerr effects, as well as mechanical strain and shape anisotropy, where the geometric shape of the propagation medium is nonsymetric.

2.1.4 Birefringence perturbations in optical fibers

All optical fibers exhibit inherent birefringence coming from small imperfections in its geometry and material properties of the fiber. These imperfections are randomly distributed along the fiber, and give rise to a position dependent birefringence vector. We model this birefringence position dependent vector as having a random orientation along the fiber. we call this inherent birefringence the static birefringence.

The polarization state in a fiber will change due to this static birefringence and any birefringence perturbations according to the equation

$$\frac{ds}{dz} = [\beta(z) + \Delta\beta(z,t)] \times s \tag{2.23}$$

Where $\Delta\beta(z,t)$ is a birefringence perturbation at a given time and place along the fiber. By constructing a rotating coordinate system such that $v'(z) = R^{-}1(z,0)v(z)$ where $dR(z,0)/dz = \beta \times R(z,0)$ we can remove the static birefringence simplifying the equation to

$$\frac{ds}{dz} = \Delta\beta(z,t) \times s \tag{2.24}$$

This rotation transform will work as a perfect compensator for the static birefringence, in the new coordinate system the polarization state of incoming and outgoing light does not change in the absence of a birefringence perturbation, that is $s(z) = s(0) = s_0$.

If we consider a small perturbation perturbation of the polarization state $\Delta s \ll 1$, we have:

$$\frac{d(s_0 + \Delta s)}{dz} = \Delta\beta(z,t) \times (s_0 + \Delta s) \tag{2.25}$$

$$\frac{ds_0}{dz} + \frac{d\Delta s}{dz} = \Delta\beta(z,t) \times s_0 + \Delta\beta(z,t) \times \Delta s \tag{2.26}$$

$$\frac{\Delta s}{dz} = \Delta\beta(z,t) \times s_0 \tag{2.27}$$

We can separate the elements due to distributivity in the cross product and differentiation operators. The terms in the final lines disappear because $\frac{ds_0}{dz} = 0$ due to the rotating coordinate system removing its z dependence, and $\Delta\beta(z,t) \times \Delta s$ due to both Δ_s and $\Delta\beta(z,t) \ll 1$.

We can then see that only the components of $\Delta\beta$ orthogonal to s_0 will affect the polarization state.

integrating over z we get:

$$\Delta s(z) = \int_0^z \Delta\beta_\perp(z,t) \times s_0 dz \tag{2.28}$$

The SOP variations we measure is the time evolution of this integral.

An important implication of this is that the polarization variation we measure will be the integral of all perturbations on the birefringence along the fiber. This means that locating where a signal originates along the fiber is impossible.[3]

2.1.5 Polarization variation mechanism

In this section we will introduce a few of the physical phenomena that cause the polarization state to change. These phenomena generate the signals we observe.

The Faraday effect

The Faraday effect is a magneto-optical effect that will rotate the polarization propagating through a media in the presence of a magnetic field along the axis propagation.

Currents in the high voltage transmission lines will induce a varying time magnetic field, $B(t) = B_0 \sin 2\pi 50t$, around wire in accordance with Biot-Savart law. The optical fiber is lashed around this power-line. A part of the magnetic field will therefore align with the fiber and contribute to the Faraday effect. This is the source of the strong 50 Hz variation we see in the signal.

The Faraday effect is given by:

$$\theta = \mathcal{V}Bd \tag{2.29}$$

where θ is the rotation angle,d is the distance traveled, B is the applied magnetic field along the direction of light propagation. $\mathcal{V}$ is the Verdet constant, a material specific constant determining how strong the Faraday effect is in a given material, it has units radians per meter per Tesla.

As the fiber is only wound around the transmission line for about 1.5 km, we consider the field static in space and its time derivative as zero for the purposes of interacting with the propagating light. This is valid as the light propagates through the entire cable on µs scale while the magnetic field oscillates at 50 Hz. The winding also causes the magnetic field to be proportional to the number of winding around the power-line and the angle of this winding helix. These are constant and can be abstracted away by including them in B_0, the constant describing the amplitude of the oscillating magnetic field.

In our case the Faraday effect will only cause oscillations around the S_3-axis, not full rotations. This is due to the combination of the cable being quite short in conjunction with only a small part

of the magnetic field contributing to the fiber and that the magnetic field is relatively weak. The fused silica in the fiber is also not particularly optically active.

It should be noted that the Faraday effect wont change the polarization Ellipcity, only rotate the ellipse. In terms of stokes parameters this means it will only change the S_1 and S_2 parameters, not S_3. In stokes space the Faraday effect can be represented as a rotation around the S_3-axis of θ degrees. [6]

Strain optic effect

The strain optic or acousto-optic effect is the phenomenon that the optical properties of a material will change when deformed. This effect gives rise to a transient birefringence perturbation when acoustic waves from nearby vibrations propagate through the fiber. This perturbation is dependent on the type of acoustic wave as well as its orientation with respect to the direction of the light propagation.

Strain is the relative displacement of particles in a material. If we define the vector $\mathbf{u} = (u_1, u_2, u_3)$ as the displacement vector at position $\mathbf{x} = (x_1, x_2, x_3)$. The strain tensor is defined as $s_{ij} = \frac{1}{2}(\partial u_j/\partial x_i + \partial x_j/\partial_j)$. Where i,j represent the axes of the Cartesian coordinate system, This tensor is represented as a 3×3 matrix. The elements along the diagonal of the matrix represent tensile strain while the other indices represent shear strain.

The strain optic effect describes how this strain tensor affects the impermeability tensor and thus the optical properties of the material. The Optical characteristics of a media are described by the electric impermeability tensor, this tensor is a function of the strain in the material. In general the strain-impermeability relationship is complicated, but by using a Taylor expansion in terms of the strain we can get a linear approximation.

$$\eta_{ij}(s_{kl}) = \eta_{ij}(0) + \sum_{kl} p_{ijkl} s_{kl} \tag{2.30}$$

Where p_{ijkl} is the photoelasticity tensor. As both the strain and impermeability tensor are symmetric, and thus permutation invariant, we can combine the i,j indices and k,l indices into the indices I and K ranging from $1, 2, .., 6$ instead of $1, 2, 3$. The encoding is given by table 2.1. The

j/i	1	2	3
1	1	6	5
2	6	2	4
3	5	4	3

Table 2.1: Mapping from pairs of indices i,j/l,k to index I/K

elements of the photoelasticity tensor are also dependent on the crystal structure of the material. For the case of isotropic materials as we will handle in this work it can be represented as a 6×6 symmetric matrix.

$$p_{IK} = \begin{bmatrix} p_{11} & p_{12} & p_{12} & 0 & 0 & 0 \\ p_{12} & p_{11} & p_{12} & 0 & 0 & 0 \\ p_{12} & p_{12} & p_{11} & 0 & 0 & 0 \\ 0 & 0 & 0 & p_{44} & 0 & 0 \\ 0 & 0 & 0 & 0 & p_{44} & 0 \\ 0 & 0 & 0 & 0 & 0 & p_{44} \end{bmatrix} \tag{2.31}$$

Where $p_{44} = 1/2(p_{11} - p_{12})$. [6]

The strain optic effect should allow us to detect events mechanically affecting the fiber, like road and rail traffic. A vehicle or similar passing by will cause an acoustic wave to travel through the ground, causing birefringence. This birefringence perturbation will then change the SOP according to equation (2.28).

2.1.6 Modulation mechanism

In this work we will explore utilizing polarization stemming from the Faraday effect to modulate the lower frequency perturbations originating from acoustic vibrations. In this section we will give a short reasoning for why we should expect to see such a modulation effect.

Modulation is a nonlinear phenomenon arising from the product of two oscillations. The simplest example being the amplitude modulation from the product of two oscillations.

$$\sin(ax)\sin(bx) = \frac{1}{2}(\cos((a+b)x) - \cos((a+b)x)) \tag{2.32}$$

In our data we can observe one light wave that is affected by external sources in two different ways, the strain optic effect and the Faraday effect.

To make plausible that modulation can occur in the polarization we can observe how the strain optic effect and Faraday effect will affect a light wave when acting simultaneously in an idealized case.

The Faraday effect will rotate the polarization, in accordance with Jones calculus we get

$$\begin{bmatrix} A'_x \\ A'_y \end{bmatrix} = \begin{bmatrix} \cos(\theta) & -\sin(\theta) \\ \sin(\theta) & \cos(\theta) \end{bmatrix} \begin{bmatrix} A_x \\ A_y \end{bmatrix} \tag{2.33}$$

where theta is the rotation angle given by the Faraday effect as $\theta = \mathcal{V}BL$, in the case of the magnetic field from an AC current we get an oscillating magnetic field, $B = B_0 \sin(2\pi 50t)$. The power line will then act as an oscillating polarization rotator with frequency 50 Hz.

The strain optic effect affects light differently depending on the type and direction of the acoustic wave. As the purpose here is to demonstrate that modulation occurs we will use the simple case of a shear wave in the x-direction, traveling along the fiber in the z-direction. This wave gives a strain tensor where all elements are zero except $s_{13} = s_{31} = S_0 \cos(\Omega t - qz)$, where Ω is the acoustic frequency and q the acoustic wavenumber. In accordance with (2.30), the elements of the impermeability tensor then become

$$\eta = \begin{bmatrix} \frac{1}{n^2} & 0 & p_4 4 S_0 \cos(\Omega t - qz) \\ 0 & \frac{1}{n^2} & 0 \\ p_4 4 S_0 \cos(\Omega t - qz) & 0 & \frac{1}{n^2} \end{bmatrix} \tag{2.34}$$

Calculating the resulting refractive indices we get

$$n_1 \approx n + n^3 p_4 4 S_0 \cos(\Omega t - qz) \tag{2.35}$$

$$n_2 \approx n \tag{2.36}$$

$$n_3 \approx n - n^3 p_4 4 S_0 \cos(\Omega t - qz) \tag{2.37}$$

As an additional simplification we can assume that the light in the fiber travels so much faster than the acoustic waves that we can consider the wave a stationary oscillation.

As we assume the fiber is oriented along the z-axis, the $n_3$component will cause the same phase delay for both polarization states. We can therefore disregard it. The two components of the **E**-field are given as

$$\mathbf{E}_x = A_x \cos(\omega t - k(t)z) \tag{2.38}$$

$$\mathbf{E}_y = A_y \cos(\omega t - kz) \tag{2.39}$$

Where $k(t) = \left(n + n^3 p_4 4 S_0 \cos(\Omega t)\right) = k_0$, and $k = k_0 n$. After the polarization rotation from the Faraday effect we get

$$\mathbf{E}_x = \left(\cos\left(\theta(t)\right) + \sin\left(\theta(t)\right)\right) A_x \cos(\omega t - k(t) z) \tag{2.40}$$

$$\mathbf{E}_y = \left(\cos\left(\theta(t)\right) - \sin\left(\theta(t)\right)\right) A_y \cos(\omega t - k z) \tag{2.41}$$

We now have the product of two oscillations, giving rise to an amplitude modulation.

2.2 Signal processing

In this section we will give a brief overview of the frequency domains we expect to find, and a short overview of the theory behind the signals processing used in this work.

2.2.1 Spectrograms and frequency overview

Different signal sources have distinct frequency profiles as indicated in table 2.2. This table is based on the work done by Jordi et al. in [7] where a seismograph was placed in downtown Barcelona to record the seismic activity in the city center. We expect the SOP signal to exhibit a similar spectrum by way of the strain optic effect, thus we base most of our frequency regions of interest on this information.

The main tool used in the signal processing was the spectrogram. A spectrogram is a signal processing technique for studying the time evolution of the frequency spectrum of a signal. Spectrgrams are constructed by partitioning the data into equal length segments, taking the Fourier transform of these segments and plotting the Fourier transformed segments in a colormap with time on the x-axis and frequency on the y-axis. We can think of this as a matrix like seen in (2.42). In this matrix $S_i(t_k)$ is the i-th bin of the discrete fourier transform of the k-th segment.

Source	frequency Domain[Hz]
Power grid	49.9-50.1
Anthropic seismic signals	1-35
Peak road traffic signal	8-12

Table 2.2: Table of frequency domains of interest.

$$\begin{bmatrix} S_N(t_0) & S_N(t_1) & \cdots & S_N(t_K) \\ S_{N-1}(t_0) & S_{N-1}(t_1) & \cdots & S_{N-1}(t_K) \\ \vdots & \vdots & \ddots & \vdots \\ S_1(t_0) & S_1(t_1) & \cdots & S_1(t_K) \\ S_0(t_0) & S_0(t_1) & \cdots & S_0(t_K) \end{bmatrix} \tag{2.42}$$

When utilizing spectrograms there are several parameter that must be chosen, first we need to choose a segment length. Next we need to chose the spacing between the starting points of the segments. In many cases it is desirable to have some overlap between the segments. The frequency resolution of the spectrogram is given as a function of the sampling frequency of the signal and the number of samples in a segment. For all analysis except the train detection scheme described in 3.3.4 we chose to use 1 minute segments with a spacing of 1 minute, that is no overlap. the frequency resolution of 44.1 kHz on 1 minute segments calculates to 0.01666.

A core premise in our analysis is that different activity along the fiber will have distinct frequency signatures the that manifest in the polarization variation. Another premise is that different sources will be more or less prominent at different times. The reason for using a spectrographic approach in this work was that it allows us to simultaneously look for patterns in both time and frequency.

Another key advantage of utilizing specrograms is that it is maintains the interpretability of the data and the results. In this work we are looking to detect and characterize events. To this effect maintaining a degree of interpretability is desireable.

2.2.2 SSA

In part of analysing the sidebands depicted in 4.7 we also used singular spectrum analysis(SSA). This apporach was chosen because it allows us to effectively detrend a signal with nonpolynomial trend. This allowed us to extract only the oscillations in the signal.

SSA is a decomposition based time series analysis algorithm. The idea is to embed a time-series into a matrix and then performing a singular value decomposition on the matrix. We can then use the decomposed matrix to analyze the time-series. The first step of the algorithm is to embed the time-series $x(t)$ of length N into a matrix. First chose a window length $1 < L < N$, and define $K = N - L + 1$. We then generate a trajectory matrix, this is a $L \times K$ matrix where the i-th column consist of the time-series elements $x(i)$ to $x(i + L)$. The matrix looks as follows:

$$X = \begin{bmatrix} x(0) & x(1) & \cdot & x(K) \\ x(1) & x(2) & \cdot & x(k+1) \\ \vdots & \vdots & \ddots & \vdots \\ x(L) & x(L+1) & \cdots & x(N) \end{bmatrix} \tag{2.43}$$

A key thing to note here is that the matrix is a Hankel matrix, a class of matrices characterized by the fact that all the anti-diagonals contain the same value. This is the key characteristic allowing us to interpret the matrix as an embedded time-series in this context.

We then do a singular value decomposition on the matrix to obtain the decomposition $U\Sigma V*$. U and V are unitary complex matrices with size $L \times L$ and $K \times K$ respectively. Σ is a $L \times K$ diagonal matrix with real values σ_i called singular values on the diagonal. The set $\{U_i, \sigma_i, V_i\}$ represent the i-th row of $UandV^*$are called the singular vectors, taken with the i-th singular value they form the i-th eigentriplet.

By taking the outer product of the two singular vectors and weighing it by the singular value we get $X_i = \sigma_i U_i \otimes V_i$, where $\otimes$ denotes the outer product of the vectors. X_i is a $L \times K$ matrix called the i-th singular spectrum component.

These spectrum components are then grouped based on the users choice to extract various features. The components are in decaying order of feature prominence, the first component might describe the trend of a time series, the second a large variation, while last components will predominantly describe noise. In our case we used each component independently. Mathematically the components are grouped by adding together their singular spectrum components, generating a group matrix.

After grouping each of the groups are Hankelized, where we take the average over all the anti-diagonals in the group matrix. This generates a matrix with the same structure as the original embedding matrix. We then choose which groups to include and sum the groups of interest. The new time series is extracted of along the top and rightmost edge of this final matrix. [8]

Chapter 3

Methods

This chapter will cover the methods used to enquire each of the research questions. It will also cover the sensor setup and mode of operation as well as the structure of the dataset and the preprocessing and signal processing schemes utilized.

3.1 The measurement setup

The sensor system consist of three major components, the fiber, the sensing instrument and the light source.

The sensing instrument consist of a polarizing beamsplitter that splits the beam into 2 orthogonally polarized beams. The beams correspond to $|A_x|^2$ and $|A_y|^2$. We define the coordinate system of the polarization with respect to this polarizing beamsplitter. These beams are directed onto photodiodes to record the intensity of the x and y components. The electrical signals from the photodiodes are then amplified, sampled and stored using an ADC. The amplifiers are AC coupled, with a cutoff at 0.35 Hz, to allow for a larger dynamic range. The coupling has a cutoff around 0.2 Hz. The sensor has a polarisation dependent sensitivity as we can only detect the orthogonal projection of the full SOP along the S_1 axis. This gives a relative sensitivity similar to the one for the polarizing beamsplitter in [4], given by

$$\frac{1}{2}\left(\sin^2(2\chi) + \sin(2\psi - 2\chi)^2\right) \tag{3.1}$$

where 2ψ and $2\chi$are the polar and azimuth angles describing a point on the Poincaré sphere. Similar instruments have proven effective in [4, 5].

The data are stored in 24 bits per sample FLAC files with the amplitude in each of the stereo channels corresponding to the intensity of each the two beams. FLAC is the *Free Lossless Audio Codec*, an audio encoding method for storing audio data losslessly. As polarization variations and audio are both in waveforms this encoding scheme should work well.

The fiber is as mentioned a single mode fiber. It conforms for our intents and purposes to the ITU standard [9] for single mode fibers. The fiber is located in Sarpsborg. It starts near Sarpsborg train station where the fiber is dug underground along the train tracks before diverting to follow a suburban road. After about 4.5 km underground along road and rail tracks, the fiber is undug and lashed around a high voltage air suspended power transmission line. This power-line terminates at Hasle Trafo where the sensing node is also located. The cable is exposed to the environment for about 6km. At the measurement node the fiber is sent through 20 km of dispersion compensating fiber(DCF). DCF is a fiber engineered to have an opposite dispersion relation from the rest of the fiber, this dispersion compensation occurs in a remote temperature regulated room. The signal is then diverted into a fiber optic node where an optical multiplexer copies the signal into the SOP

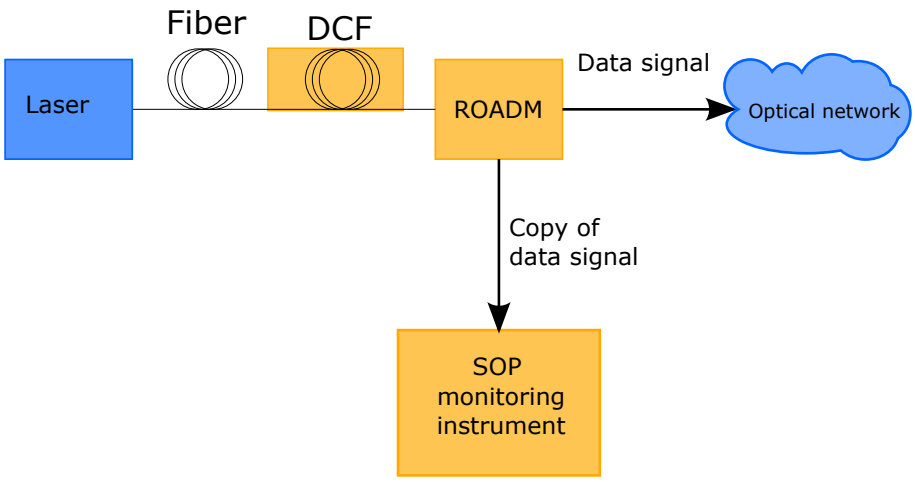

Figure 3.1: An overview of the Sensor system. The light first travels trough the fiber buried and lashed around the power line, then at the measurement node it travels through 20 km of dispersion compensating fiber before being copied at a network node and measured.

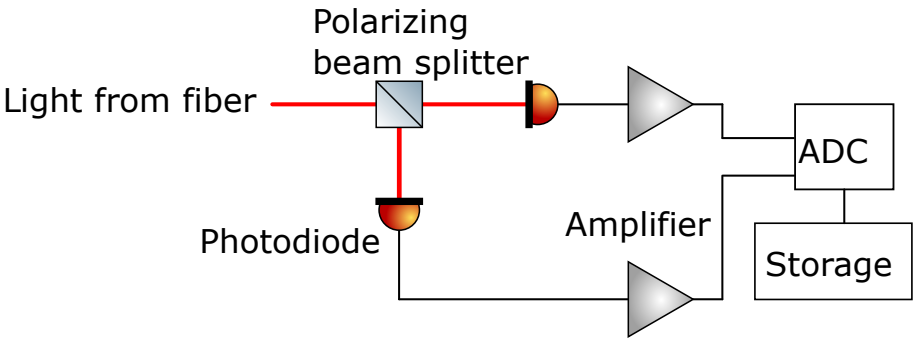

Figure 3.2: Schematic of the SOP sensing instrument. The copied signal from the network node enters the instrument, is split into two orthogonally polarized beams and measured at the photodiodes. The electrical signals are then further processed.

sensing instrument.

The laser source is a common telecommunication system, using a 10GB/s on/off keying modulation scheme. The encoding scheme is designed to keep the laser about 50% on and 50 % off. The signal as observed by our instrument then looks like a constant intensity light-source as the modulation is orders of magnitude faster than the sampling time of the sensing instrument.

3.2 Dataset

The dataset consists of a series of one minute long segments of FLAC audio files. The Stereo channels correspond to $|\Delta A_x|^2$ and $|\Delta A_y|^2$ respectively. This allows us to detect the two first of the 4 Stokes parameters in (2.20). Each one minute segment is sampled at 44.1 kHz with a 24 bit/sample resolution. A full month of data is about 240GB.

We analysed data for the entire calendar months of December 2023 and March 2023. This allows us to have two causally independent data sets, enabling us to verify any inference made by cross referencing another time period.

3.3 Signal Processing

In this section we will cover the preprocessing as well as the signal processing done to address our research questions.

3.3.1 Preprocessing

The dataset as it stands unprocessed is far too large to handle effectively. We chose to filter the data by downsampling the data from 44.1 kHz to 210 Hz. This limits the bandwidth of our study significantly, it was deemed an acceptable trade-off, as a consequence we focused our analysis on very low frequency features and phenomena.

Downsampling was executed in a standard way using the Scipy library's *decimate* function. The function operates by creating an order 8 Chebychev anti-aliasing filter and then keeping every n-th sample. In accordance with the recommendations from the Scipy documentations the downsampling was done in stages, the factors chosen were: 2,3,5,7. Some of the segments were longer than 60 seconds, we chose to simply cutoff all signals at 60 seconds to ensure data uniformity. After compressing, the data only takes 8 GB per month. This compression is not a 1-1 with the downsampling factor as post compression we save the files in Numpy arrays, these are not as compressible as the FLAC files. The data-set is still very large, however it is now small enough to be processed on a normal computer with 16 GB of RAM. The data was saved in an array with $\Delta S_0 = |\Delta A_x(t)|^2 + |\Delta A_y(t)|^2$ and $S_1 = |\Delta A_x(t)|^2 - |\Delta A_y(t)|^2$ in each row.

In order to identify the source of a signal we need some more information than what is contained in only the signal. Most things that could affect the polarization in an urban environment has an expected frequency signature, 50 Hz is strongly associated with the electrical grid, while the range 1 Hz to 35 Hz is associated with antropic sources from a seismological perspective [7]. Outside of this strict perspective it can also be associated with other effects like weather and electrical interference not stemming from the electrical grid. The core premise of the analysis approach is that if sources have distinct frequency signatures it could allow for identification of sources by using their frequency signature.

There are several with events like lightning strikes, that are associated with frequencies in the kiloHertz range. In part of our downsampling and methodology we have chosen not to focus on analysing events like this.

Further we use complimentary information like power-grid data, expected rush-hours and train

schedules to predict when we expect a given source to be more prominent in the data. A spectrographic approach allows us to observe the time evolution of the signal at a given time allowing us to take advantage of both the temporal and spectral information.

With our compressed data being limited to 105 Hz bandwidth, we chose to focus on the 50 Hz signal coming from the power grid. An interesting approach is to try using it as a modulation carrier for lower frequency signals. We chose to define the 50 Hz signal as the frequency range $49.9 - 50.1$Hz, this range is the accepted normal variation of the Norwegian power grid. We implemented these frequency range cutoffs by using an index mask, that is a Boolean array for indexing based on the frequencies of interest. We further defined the sidelobes as the range from 30 Hz to 70 Hz excluding the 50 Hz signal.

3.3.2 SOP sensing for current detection

As the fiber is lashed around a power-line we attempted to sense the total power transfer in the power-line. Magnetic fields induced by the currents in the power-line should cause a very strong 50 Hz. Accurate transmission data for individual power-lines is kept secret. We therefore used proxy data. The best proxy data publicly available is Statnett's public power-grid information [10], we tested both production/consumption data and import/export data. This data was available with hourly resolution. Our analysis consisted of the following: We observed the 50 Hz signal across an entire month. We grouped this signal by the hour and take the average over each of these segments giving an hourly average 50 Hzsignal. As the power-grid data and polarization signal now have the time resolution a meaningful correlation can be calculated. A positive correlation between import/export and production/consumption and 50 Hz signal is then expected.

3.3.3 Detection of traffic

In order to use SOP sensing to detect traffic we looked at the frequency bands most closely associated with human activity and road traffic. According to Jordi et al. (table 2.2) this is the range of 1 Hz to 35 Hz for general human activity, with 8 Hz to 12 Hz containing peak road traffic data. We compared the average energy in these frequency ranges with different times throughout the day. One hypothesis was that we would be able to detect the increase in traffic during rush hours, or a day and night change. Rush hour was defined as 0600-0800, and 15-18. While nighttime was defined as 2300-0500. This was done over a month long measurement campaign.

We also attempted utilizing the modulated signal around the 50 Hz signal for detecting traffic. We utilized a similar approach to the approach described above except we focused on the same signals modulated by the 50 Hz signal.

3.3.4 Detection of Trains

The fiber starts near Sarpsborg train station, as such it is reasonable to expect that the coming and going of trains will cause large vibrations in the ground. Train schedules are publicly available with minute resolution [11] allowing us to focus the analysis at the scheduled arrival and departure of trains.

We looked at the train traffic on the March 1st. As this was a normal Wednesday we expect train traffic to operate normally. In order to analyze the train traffic all arrival and departure times on the 1st were extracted from in Banenor's schedule[11]. For each scheduled train through Sarpsborg station a corresponding 10 min segment from the data was extracted based on what sixth of the hour the train was schedule to arrive at. That is if a train is scheduled at 00:3X, data from 00:30 to 00:40 was analyzed. This windowing approach was done due to convenience in extracting these segments of data. The analysis consisted of both spectrographic and time-domain inspection. In the time domain we used 5th order butterworth bandpass filters applied in both directions. The pass bands for the filters were set at 1-35Hz,1-10Hz, 8-12Hz and 20-40Hz.

These bands were chosen based on observations by the initial spectrographic analysis, as well as seismographic characterizations of subway activity in [7]. This should allow us to observe both time and frequency domain characteristics of the train passages.

For the spectrographic approach we used a slightly different approach compared to most of the other experiments conducted. First the the data was downsampled to a sampling frequency of 90 Hz, compared to the 210 Hz sampling frequency in most of our analysis. This was done to remove the 50 Hz signal as it was of no interest in this more narrow analysis. The spectrograms were constructed using 4 second windows with 2second overlap. This was done to capture shorter transients. Trains were not expected to generate sub-Hertz signals, as such the short window length was not detrimental to the train detection scheme.

3.3.5 Using the 50 Hz signal as a carrier wave

The sidelobes were analysed using log-scale spectrograms. The sidelobes cover a wide frequency range. We expect to find several different signals from different sources. Spectrograms allow us to fingerprint the frequency characteristics of these signals. The spectrograms were generated by taking the Fourier transform of each 1 minute segment and then plotting these spectra as contour plots with time and frequency on the x and y axes.

As the modulating 50 Hz signal changes drastically in strength the modulated signal will also change in strength. As the sidelobes are the signal of interest we normalize with respect to the 50 Hz signal in order to compensate for the varying carrier wave. This should give all modulated signals in the sidelobes an equal energy independent from changes in the 50 Hz signal, as well as reveal some of the signals that are modulated by the 50 Hz signal when it is weaker.

3.3.6 Other signals of interest

The most interesting signal found in sidelobes was a collection of 5-6 bands at between 68 Hz and 71 Hz. The strongest of these bands was examined by extracting the maximum from a tight region around the band. This allowed the signal to be analyzed further. We detrended the data using Singular spectrum analysis (SSA), the first component corresponds to the trend in the data, by then analysing the second component which corresponds to the largest oscillations we could estimate the frequency of the oscillations in the bands, as well as calculate the spectrogram to look at the time evolution of the frequency.

Chapter 4

Results

4.1 SOP for Current sensing

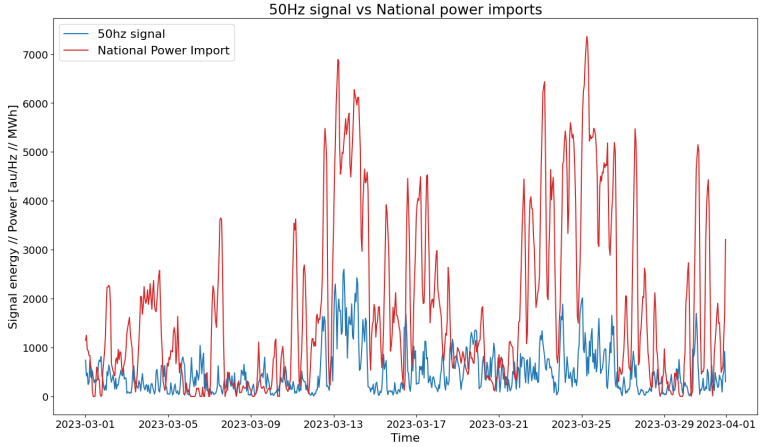

Figure 4.1: 50 Hz signal against national imports in march. Notice how the power imports and the 50 Hz signal increases around the 13-th.

Comparing the 50 Hz signal with the national power import in fig 4.1 we can see an apparent positive correlation between the strength of the 50 Hz signal and the national energy imports. Particularly starting on the 13th. Hasle trafo, where the cable terminates is one of the main junctions between the Norwegian and Swedish power grid, the increased signal likely stems from imported power from Sweden traveling through the power line.

In figure 4.2 we can see the results of comparing with the power balance, that is the production minus the consumption. When there is a negative balance the 50 Hz signal rises. This is consistent with our observation that the energy in the 50 Hz signals are related to imports, as the deficit in production must be accounted for by imports.

Power imports-50 Hz correlation in March	0.513
Power import-50 Hz correlation in December	0.517
Power Balance - 50 Hz correlation in March	-0.49

Table 4.1: Correlation coefficients for power grid data and 50 Hz signal

The correlation coefficients are tabulated in table 4.1. In the table we can see that the correlation is only 0.5. Usually a correlation above 0.7 is considered a strong correlation, we fall short of

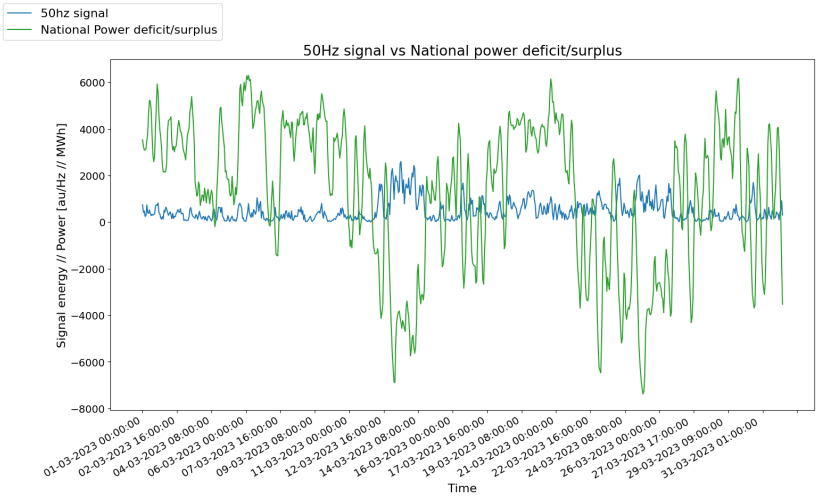

Figure 4.2: The graph illustrates the national power balance compared with the 50 Hz signal. We can again note the large deficit around the 13th, and accompanying increase in 50 Hz signal

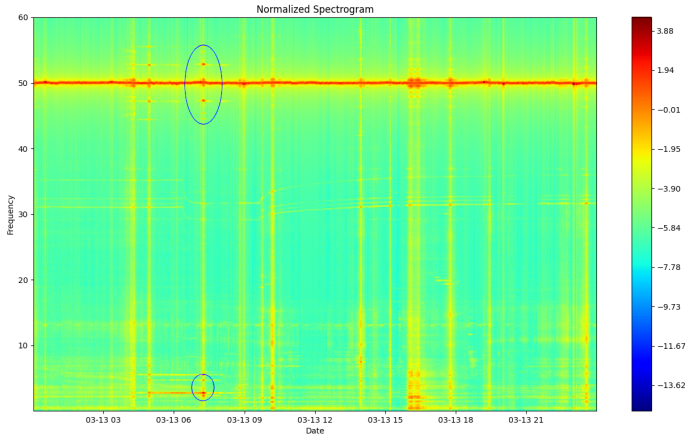

Figure 4.3: Spectrogram of Monday March 13-th. The highlighted lobes around the 50 Hz signal are modulated up from the highlighted 2 Hz signal.

that threshold. This is likely due to the fact that the power-grid data is a proxy measure of the current in the power-line. The power-grid data is national, as such it includes a lot of data that is not related to the specific import point we observe. Further the power-line measured does not carry all the imports going through Hasle, it is part of the network distributing power from the substation further west. We expect a tighter correlation if we had access to the actual current traveling through the fiber.

4.2 Using the 50 Hz signal as a carrier wave

We also examined the possibility of using the 50 Hz signal as a carrier wave being modulated by lower frequency signals. In 4.3 we can see that the 50 Hz is modulated by a 2 Hz signal. This proves the pressence of amplitude modulation in the signals as a phenomenon. The 2 Hz signal has not been attenuated and is still available for processing.

The modulated signals were affected by the changing 50 Hz signal energy. An attempt to compensate for this by normalizing with respect to the 50 Hz signal. This compensation scheme helped

mitigate the 50 Hz influence however it did not fully compensate for the influence as we shall see in the next section. Plots of the sidelobes and the efficacy of normalization on a month scale can be found in appendix A.

4.3 SOP Sensing for Traffic Monitoring

We investigated the possibility of using the fiber optic cable to monitor both road and rail traffic. In this section we will cover our results on utilizing the technology for monitoring road and rail traffic.

4.3.1 Road Traffic Monitoring

We start by monitoring the frequency ranges associated with road traffic and general human activity over the entire month.

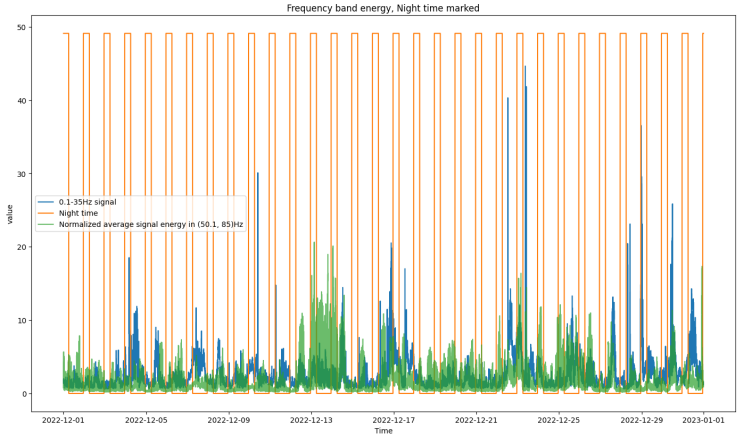

Figure 4.4: The 0.1-35 Hz average signal over an entire month in blue, with night time marked. The green line is the 50.1-85 Hz modulated signal. In the modulated signal we can see influence of from variations in the 50 Hz.

Figure 4.4 show the average signal in the 0.1-35Hz range over an entire month. We can see that that the energy is distinctly lower in the nighttime compared to the daytime. Further we can see that the 50 Hz signals changing energy affects the modulated signal.

Frequency	Night time percentage	Rush hour percentage
Percent of time period	29.9 %	17.7%
Percent of 0.1-35Hz signal	26.6 %	16.87%
Percent of 8-12Hz signal	26.3 %	16.7%

Table 4.2: This table compares the percent of time night time and rush hours with the portion of energy in the signals during rush hour and at night.

In table 4.2 we can observe the time distribution of the signal energy across the measurement period. Note the 3 % discrepancy in the time vs signal energy percent druing the night. This supports that these signals are related to human activity or traffic of any type as anthropic activity is reduced at night. For the rush hours the difference is only 1 % lower, to detect the increased rush hour traffic volume we would have expected a larger difference, and an increase in the signal energy not a decrease as we see here. The 1 % rush hour difference is so small that it can likely be attributed to random variation.

4.3.2 Train traffic Monitoring

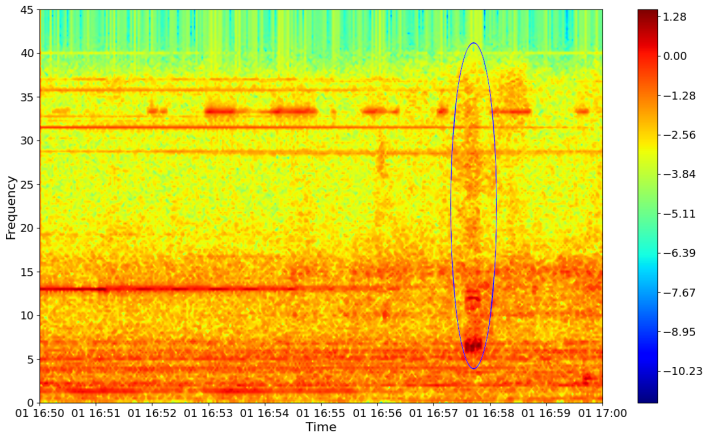

Figure 4.5: Detection of a train scheduled for departing at 16:57. We can see a broadband increase in energy between 6-40Hz between 16:57:30-16:57:50.

Train traffic is visible in both the time and frequency domains. In figure 4.5 we can see the a detection of a train passage highlighted. In the frequency domain the train is visible as a broad increase in energy between 6-40Hz, the signals are strongest in the 6-7Hz range. The train passage is a short transients lasting less than 20 seconds. This 20 second duration is consistent with the time a train takes to break, it is therefore possible these signals are closely related to the train braking as it arrives.

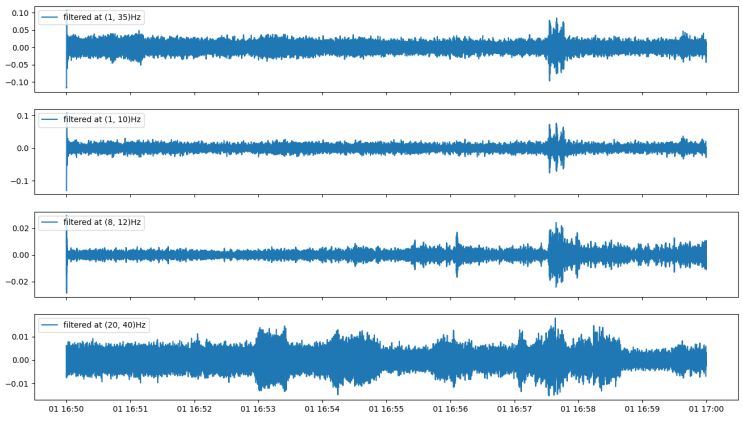

Figure 4.6: Time domain train passage signal. The top Note the clear peaks in all but the 20-40Hz signal.

In the time domain we can see the train passing particularly clearly in the 1-10Hz range. In the 20-40Hz region the train passage is not as distinctly visible as the in the lower freqeuncies. Further work is required to fully understand both the 20-40Hz and the lower frequency signals. we do not know what parts of the train passage process are associated with various frequencies.

There are is a large variation in the characteristics of a train passages, figure 4.5 depicts a particularly clear detection, in appendix A further examples demonstrate the large variance in train detection signals. This decreases the confidence in our detections, with further work a clearer characterization and understanding of these signals could lead to a confident and robust system.

Some trains are also missed outright due to off-schedule trains that arrive outside of our detection window. A slight delay even within Banenor's threshold for punctuality of less than 4 minutes could cause a missed detection due to our relatively short detection window.

4.4 Other Signals of Interest

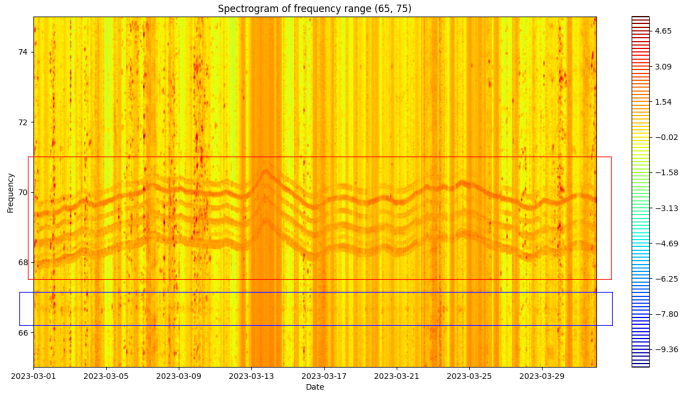

Figure 4.7: Spectrogram of the range 65-75Hz range. Highlighted we can see a group of bands. slightly below we see a faint horizontal line at 66.6 Hz highlighted by a blue rectangle.

In 4.7 we can see a group of frequency modulated bands highlighted at around 70Hz. They drift slowly in frequency. They also modulate their frequency with a peak to peak frequency-modulation of 0.1 Hz with a stable period of 30 minutes. The intensity of the bands peak is relatively constant between 0-10 dB/Hz except for a few peaks caused by event that overlap with the frequency bands.

Just below the frequency bands, we can see a steady 66.66 Hz signal. This steady signal is also visible in figure 4.8 with a steady 33.33 Hz. This indicates that a 16.66 Hz signal has been modulated by the 50 Hz signal. This frequency coincides with the power delivery frequency of the rail network, which operates on a 16 kV, 16.66 Hz system [12].

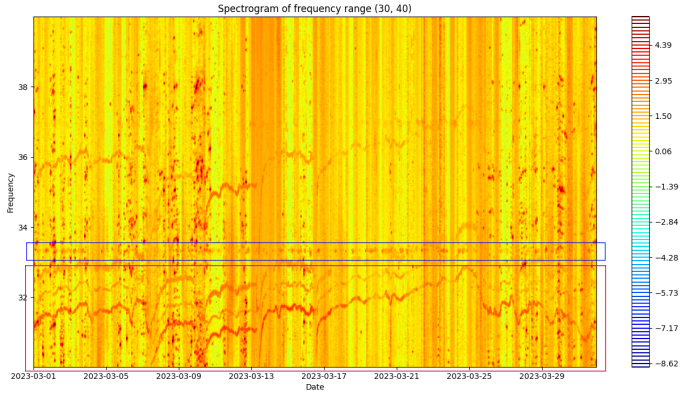

Figure 4.8: Spectrogram of the 30-40Hz range. First, in the lower highlight box, note the frequency bands similar to the ones found in the 70 Hz region. Another feature to note is the highlighted line at 33.3 Hz

On the lower sidelobe, fig 4.8 we can see a similar signal, with a group of bands seeming to drift around 32 Hz.These signals are similar to the signals in the 70 Hz region, in that they are bands of frequency modulation. However they are neither perfectly mirrored nor perfectly doubled as we

would have expected from a modulated or harmonic signal. This could be due to distortions as the frequency band around the 32 Hz, this is significantly more noisy than the relatively quiet 70Hz region.

The origins of the signals remain unknown. A theory is that they are related to regulation system in a nearby industry or a power-plant, however we have not been able to conclusively identify any plausible source. Another possible source of the bands could be due to an internal combustion engine near the fiber. There are some indications that the bands can be the result of amplitude modulation. If we assume that the signals are modulated then the corresponding base frequency for the bands should be between 18 Hz to 21 Hz, corresponding to an rpm of 1080 rpm to 1260 rpm. If the bands are not modulated then the frequency of around 70 Hz would correspond to RPMs around 4080 to 4260, both of these RPM ranges are well within what could be expected from an internal combustion engine.

Chapter 5

Discussion

We can detect peak currents in the power-grid
Using 50 Hz as carrier wave has some limited potential
There is potential to detect traffic, especially train traffic

Table 5.1: Key findings

5.1 Is it possible to detect current peaks in the powergrid?

There exists a correlation between power imports and the 50 Hz signal as tablulated in 4.1. Hasle Trafo is one of the main import junctions from Sweden. The power line this fiber is lashed around goes westward from Hasle. The power line therefore will not carry all the south Swedish imports. This along with the fact that the power-grid data is covers all national imports goes far in explaining why we only see a weak correlation. These detections indicate that SOP sensing could have some potential for monitoring currents. Much of the reason why detecting currents works so well is that the 50 Hz signal is very strong and its source is unambiguous.

5.2 Is it possible to detect traffic

Detection of rush hour traffic is significantly more difficult. By monitoring the lowest parts of the spectrum as well as the modulated modulated signals in the sidelobes we attempted to detect road traffic. This approach proved ineffective in detecting rush hour traffic. This does not necessarily mean that the data does not contain any information about road traffic.The lack of during rush hour traffic detections, could be due to the fact that while traffic volume,i.e the amount of cars on the road, are at their highest during rush hour, the average velocity of cars is at its lowest. The amplitude of the vibrations a vehicle generates are related to both the mass and the velocity of the vehicle. A large amount of slow moving cars do not necessarily generate a large signal.

While we have not been able to make a conclusive detection of road-traffic, we can to a certain extent use the SOP signal in the 1-35Hz frequency range as an activity proxy. For some purposes distinguishing what type of activity is not necessary, only detecting anomalous activity. With further development of signal processing it could be possible to make more specific detections. An approach to achieve this would be to do controlled tests to get verified detections that can then be matched to data as seen in the field to detection.

Train detections proved quite effective, this was likely helped by the fact that trains generate large vibrations, and that they follow a predefined schedules. The fiber is also located close to the tracks increasing our sensitivity. There is a large variation in train traffic signals, a few examples can be seen in appendix A. Further work is required for interpreting these signals. Some off-schedule

trains are so delayed they arrive outside the detection window. Broadening the detection window would likely have helped in this regard.

Trains braking is likely the loudest parts of the train passage process. The signals we see could be caused by the power transfer in to the rails. Brake screech is also a major source of noise, however brake screech occurs in the kiloHertz range, as such this effect is not visible in our data, however further work could leverage brake screech as well. The goal set out was to determine whether there is potential for using the measurement technique for train monitoring, which there appears to be.

Comparing our results to the earlier work in [5] and [4] a key difference seems to be that we do not have any particular high sensitivity points along the fiber. This seems to particularly affect the detection of traffic, this was quite successful in [5]. They utilized a quite different approach compared to this work. They used a fiber in downtown Torino, and were able to detect distinct spikes separated by a few tenths of a second as the axles of cars passed over high sensitivity spots like the trenches where the fibers are burried. Our fiber is not known to have the same high sensitivity points. However testing this approach in conjunction in conjunction with analysis or controlled experiments to distinguish road traffic from other transients like train traffic.

5.3 Is it viable to use the 50 Hz signal as a carrier wave

Using 50 Hz signal as a carrier wave had some varying results. A major issue is that the amplitude of the carrier wave is not stable. This was in part mitigated by normalizing on the carrier wave amplitude, however this approach is not ideal. It was also possible to resolve and identify most lower frequency signals without the use of the 50 Hz signal, while it is an interesting approach it has proved to unstable and does not provide any significant new information to the signal.

The proof that modulation effects are present in the signal is still of value for the further study of signals in the regions close to the 50 Hz signal. The presence of modulation has implications for future analysis of SOP monitoring systems as we need to consider whether the signals are the result of modulations or not.

5.4 Evaluation of own work and methodology

The Spectrographic approach chosen allows for identification of both the time of events and their frequency characteristics. In our analysis we rely on visual inspection. This approach is limited by the contrast the signals have in the color map. Weaker and more subtle sources will therefore not be detected in this analysis.

It should be noted that the fiber optic network was not developed to be a sensing network, it is a communication network, the sensing operations done in this work are done with no disruption to the communication network.

The choice to compress the data by downsampling, while being necessary to limit the size of the dataset, has the downside that all but the most low frequency data is lost. There are signals in the higher frequency domains like lightning strikes and the screeching of train brakes, that are unavailable in this analysis, as a result of this choice. Brake screech in particular could have further augmented the detection of trains.

In the month-scale analysis we have used a 1 minute window in the spectrographic analysis. Using a Fourier transform will average the signal over the window. Events like passing trains have significantly shorter transients, this averaging, along with a longer timescale allowing for larger variations in PDS can cause short timescale events to disappear in the color map as the contrast becomes insufficient.

Another problem arising from the 1 minute windows was artifacts appearing at the edges of each minute. These artifacts appear as spikes that occur sporadically at the start and end of each 1

minute segment. The artifacts likely arise from the transient response of the anti-aliasing filters used in the downsampling process. The simplest way to mitigate this would be to use longer segments, We were chose not to use larger windows due to the large data-set as well as the database structure making 1 minute segments very convenient. These artifacts made time domain analysis very difficult. We found that these effects did not generate significant noise in the frequency domain, probably because they are such short transients. For time domain applications we found that removing the first and last few observations in in each window was effective at removing the artifacts at the cost of discarding a few milliseconds of data.

Accounting for the timevarying 50 Hz signal is also non-trivial, especially when attempting to utilize it as a . As the 50 Hz signal varies distinguishing a a variation in the modulated signal and and the carrier wave can be difficult. We attempted to counteract this by normalizing with respect to the timevarying 50 Hz signal. This should attenuate signals where the 50 Hz is large and amplify signals where the 50 Hz is weak, however this is still a post processing solution, and the modulation effect observed is not linear, as such if the 50 Hz intensity is not sufficiently large we could wind up with no signal. The lower bound of the frequencies detectable by the instrument proved to be sufficient for our applications, however this study proves the concept, and it could have useful applications in another context.

In our case we are not only operating in an underground domain. There are several other sources that could have overlapping frequency signatures like weather and electrical inference not coming form the main power grid. The fiber starts out underground where it is sensitive to vibrations from traffic, but shielded from weather effects. It is then unburried and suspended along a power line, here it is likely more isolated from traffic vibrations, but more exposed to weather effects. In our analysis we have mainly utilized frequency ranges derived from seismographic studies, the sources we have defined therefore likely have significant overlap with other sources particularly weather effects like wind and rain that we have not explored in this study.

Distinguishing between signals that are the result of amplitude modulation and signals that have original frequencies in the range can also be difficult. This can be compensated for by calculating the sum of the modulated signals, as the sum should be equal in both lobes of a modulated signal.

The data is gathered in a noisy urban environment. There is therefore a plethora of signals, but very hard to identify the source of any given signal, especially for monitoring sporadic activity like road traffic. We are however able to make some quite effective detection's when the time and frequency signature is precisely known beforehand. The major findings in this work are detecting current variations and train traffic. We know beforehand that current continuously flows in the power-grid its frequency is also very narrowly defined. For trains we can check the schedule and we can estimate the frequency ranges where we expect train traffic to occur. This knowledge of the both time and frequency characteristics proved critical in making confident detections. Further characterization of the detection signals is required to generate an automatic system.

5.4.1 Further work

The measurement technique is still nascent, we foresee further development especially in signal processing allowing for more confident and precise detection. A major challenge is fingerprinting sources. An approach to help mitigate this could be to generate a supplementary data-set of controlled events in order to use a pattern matching approach to extract the key characteristics of various sources. On the deployment side a possible circumvention of the lack of spatial resolution could be to install a SOP sensing instrument at each optical amplifier along the cable. This should allow us to distinguish between which amplifier the signal originated.

Chapter 6

Conclusion

In this work we have explored possible applications of using the fiber optic network as a distributed sensor. This was done by utilizing a polarizing beamsplitter cascade with a pair of photodiodes to measure changes in the polarization of the light in the fiber. This instrument was attached to a fiber optical telecom system located in Sarpsborg. The sensor is fully integrated into the telecom system and utilizes the telecom signal itself for sensing. The fiber was located near the train-station, along a road and lashed around a high-voltage power line. We successfully detected current surges in the power line. We were also able to detect the passage of trains along the fiber. Applications in monitoring rush hour road traffic have also been explored with more limited results. Using controlled detections to generate a template signal of traffic could be advantageous for developing the traffic monitoring potential further. The possibility of using the 50 Hz signal as a carrier wave for lower frequency signals was explored, the phenomenon is verified to exist, but further work is required to find applications. For train monitoring further work is required in fingerprinting train passages as a step to developing a more robust detection scheme. There is significant potential for further development of many of these applications.

Acknowledgements

I would like to give a heartfelt thanks to my supervisors Dag Roar Hjelme at NTNU and Steinar Bjørnstad at Tampnet for their invaluable guidance, fruitful discussions and motivation in this work.

Bibliography

1. Cantono M, Castellanos JC, Batthacharya S, Yin S, Zhan Z, Mecozzi A and Kamalov V. Optical Network Sensing: Opportunities and Challenges. *Optical Fiber Communication Conference (OFC) 2022*. Optica Publishing Group, 2022 :M2F.1. DOI: 10.1364/OFC.2022.M2F.1. Available from: https://opg.optica.org/abstract.cfm?URI=OFC-2022-M2F.1
2. Myndighet NS. Sikkerhetsfagligråd - Et Motstandsdyktig Norge. 2023 Mar 9. Available from: https://nsm.no/aktuelt/sikkerhetsutfordringene-norge-star-overfor-mot-2030
3. Mecozzi A, Cantono M, Castellanos JC, Kamalov V, Muller R and Zhan Z. Polarization sensing using submarine optical cables. Optica 2021 Jun; 8:788–95. DOI: 10.1364/OPTICA.424307. Available from: https://opg.optica.org/optica/abstract.cfm?URI=optica-8-6-788
4. Barcik P and Münster P. Measurement of Slow and Fast Polarization Transients on a Fiber-Optic Testbed. Optics Express 2020 Apr; 28. DOI: 10.1364/OE.390649
5. Bratovich R, R. FM, Straullu S, Virgillito E, Castoldi A, D'Amico A, Aquilino F, Pastorelli R and Curri V. Surveillance of Metropolitan Anthropic Activities by WDM 10G Optical Data Channels. *2022 European Conference on Optical Communication (ECOC)*. 2022 :1–4
6. Saleh BEA and Teich MC. Fundamentals of Photonics. Wiley, 2019. Chap. 10,20
7. Diaz J, Ruiz Fernandez M, Sánchez-Pastor P and Romero P. Urban Seismology: On the origin of earth vibrations within a city. Scientific Reports 2017 Nov; 7. DOI: 10.1038/s41598-017-15499-y
8. Nina Golyandina VN and Zhigljavsky A. Analysis of Time Series Structure: SSA and Related Techniques. Monographs on statistics and applied probability. Chapman and Hall, 2001
9. Characteristics of a single-mode optical fibre and cable. Standard. Geneva, CH: International Telecommunication Union, 2016 Nov 13
10. statnett. Tall og data fra kraftsystemet. Available from: https://www.statnett.no/for-aktorer-i-kraftbransjen/tall-og-data-fra-kraftsystemet [Accessed on: 2023 May 25]
11. Available from: https://www.banenor.no/togselskap/kapasitetsfordeling/daglige-rutegrafer/ [Accessed on: 2023 Jun 29]
12. A. RK. kontaktledning - jernbane i Store norske leksikon på snl.no. Available from: https://snl.no/kontaktledning_-_jernbane [Accessed on: 2023 Jun 23]

Appendix A

Supplementary Figures

A.1 Train Detection Supplemental Figures

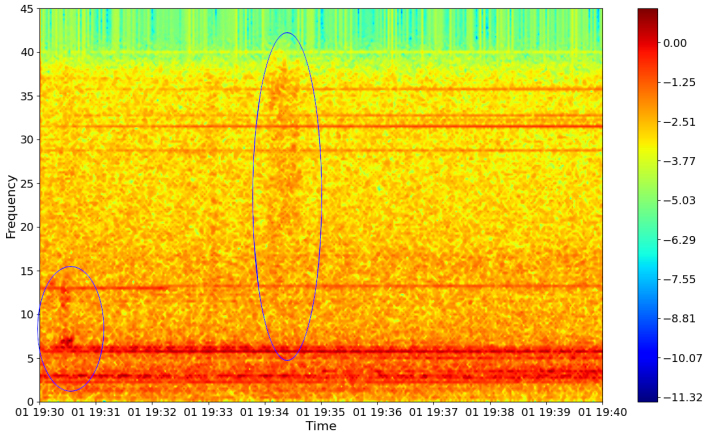

Figure A.1: Supplemental Train detection. Here we can see a peak at 6 Hz followed by a broadband energy increase in the higher frequencies above 20 Hz a few minutes later.

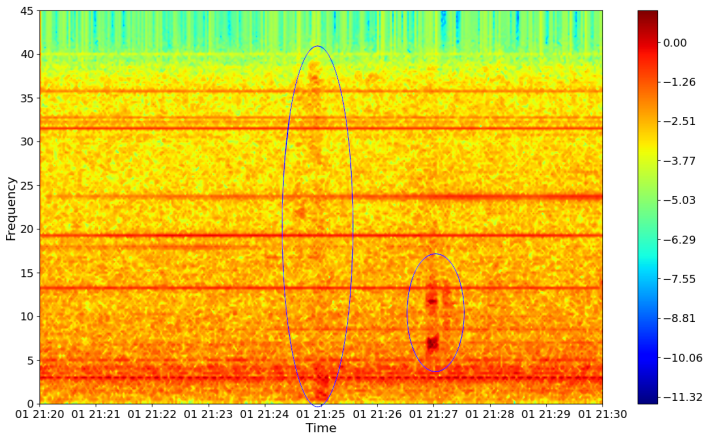

Figure A.2: Supplemental train detection. Here we cans see a detection where the lower frequency peak is below the 6-7Hz we usually see. a few minutes later a 6 Hz peak is seen

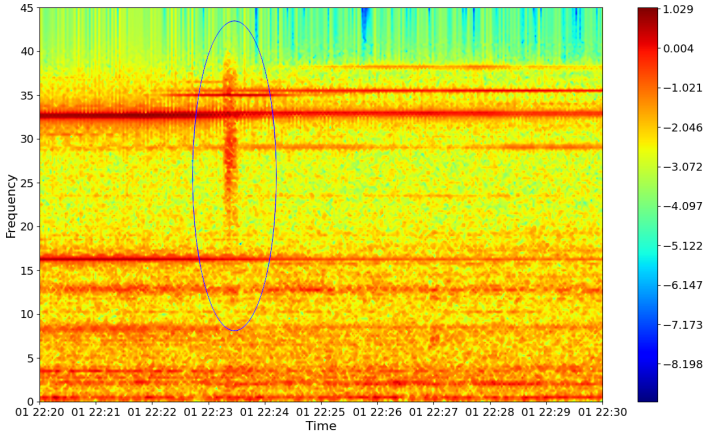

Figure A.3: Supplemental train detection. Here we can see a detection where the sub 10 Hz component is absent.

In figure A.1 we can see that the high and low frequency signals are separated in time. The interpretation of this time separation is not clear. In figure A.2 we can see that one of the detections has a much lower bottom frequency. we can however also see another peak at 6-7 . In figure A.3 we cna see what seems to be a detection however there is none of the very low frequency singal that has been strongest in other detecitons.

A.2 Current Detection Supplemental figures

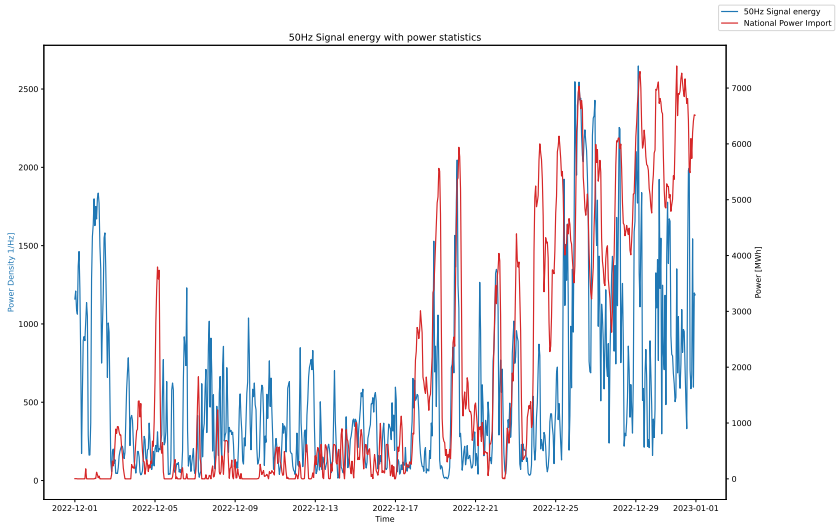

Figure A.4: 50 Hz signal compared to power imports in December

A.3 Other signals of Interest Supplemental Figures

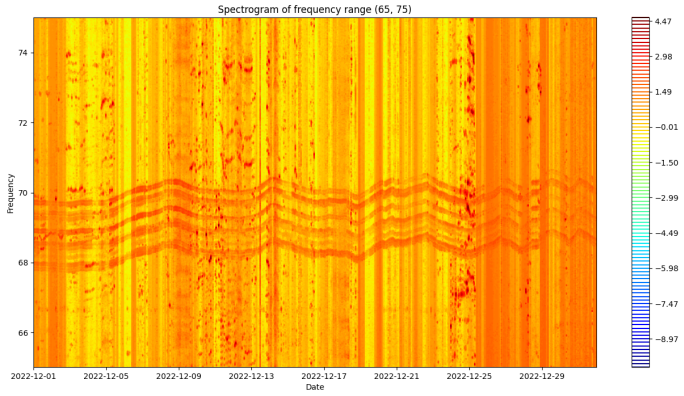

Figure A.5: 65-75Hz spectrogram for December. In this plot we can see that the 70 Hz signals are constantly present even across months.

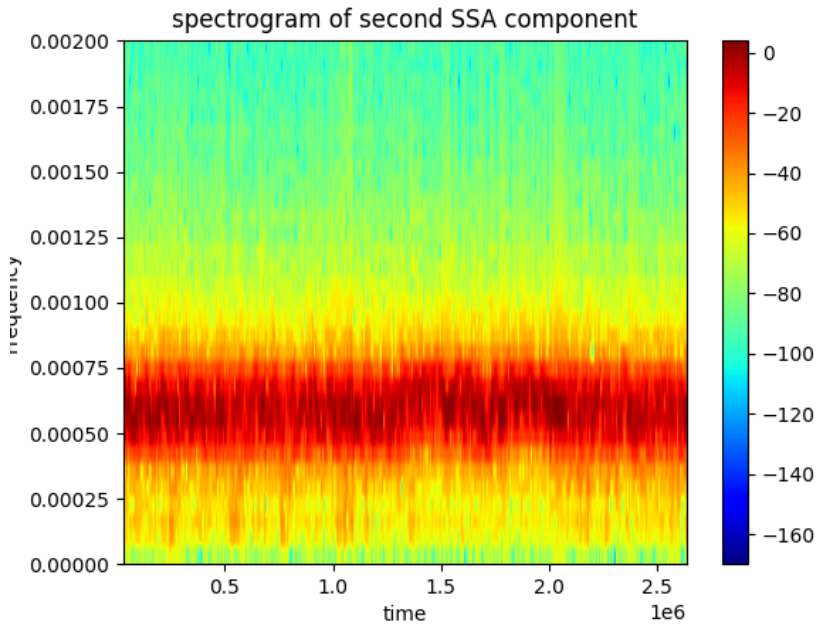

Figure A.6: Spectrogram of the second SSA component of the 70 Hz bands across the entire month. Validating that the frequency is stable.

A.4 Road Traffic detection Supplemental figures

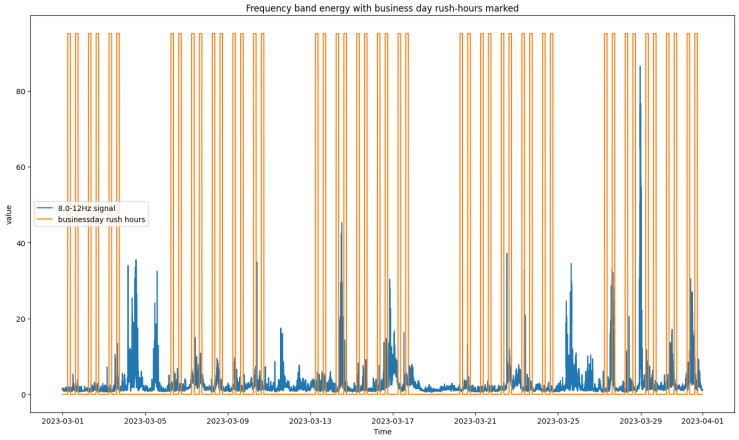

Figure A.7: The average energy of the 8-12Hz signal across an entire month with business day rush hours marked. This is the frequency band most closely associated with road traffic. We can see that the overlap with rush hours is not very significant.

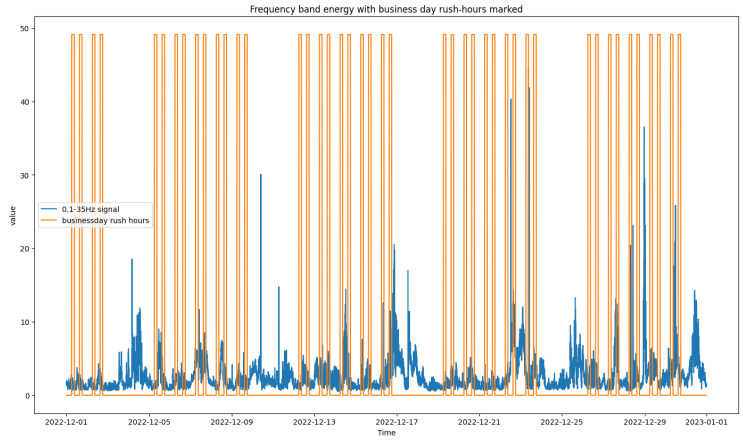

Figure A.8: 0-35Hz signal as a human activity proxy with rush hour marked.

A.5 Carrier wave Supplemental figures

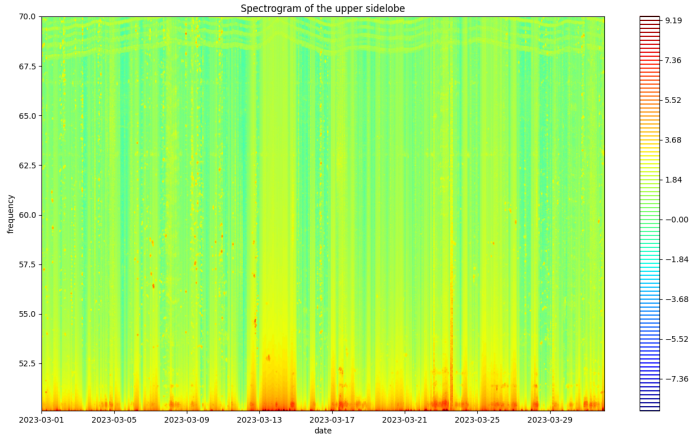

Figure A.9: The upper sidelobe in March. Here we can see that the 50 Hz signal bleeds into the sidelobes.

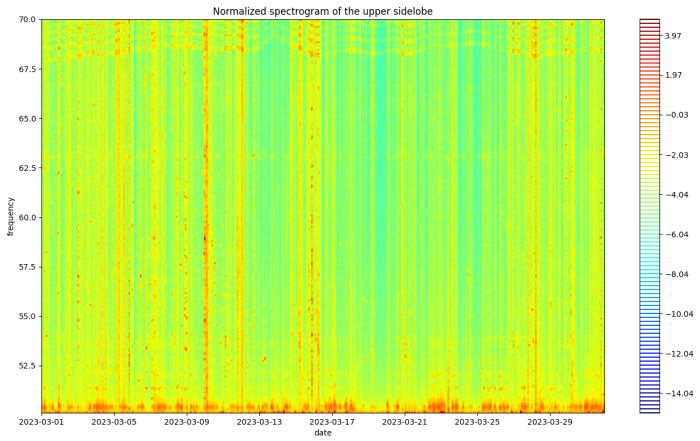

Figure A.10: The upper sidelobe in March normalized on the 50 Hz signal magnitude. Here the modulated signals are more clearly visible. We can however still see a clear influence of the varying intensity of the 50 Hz signal.

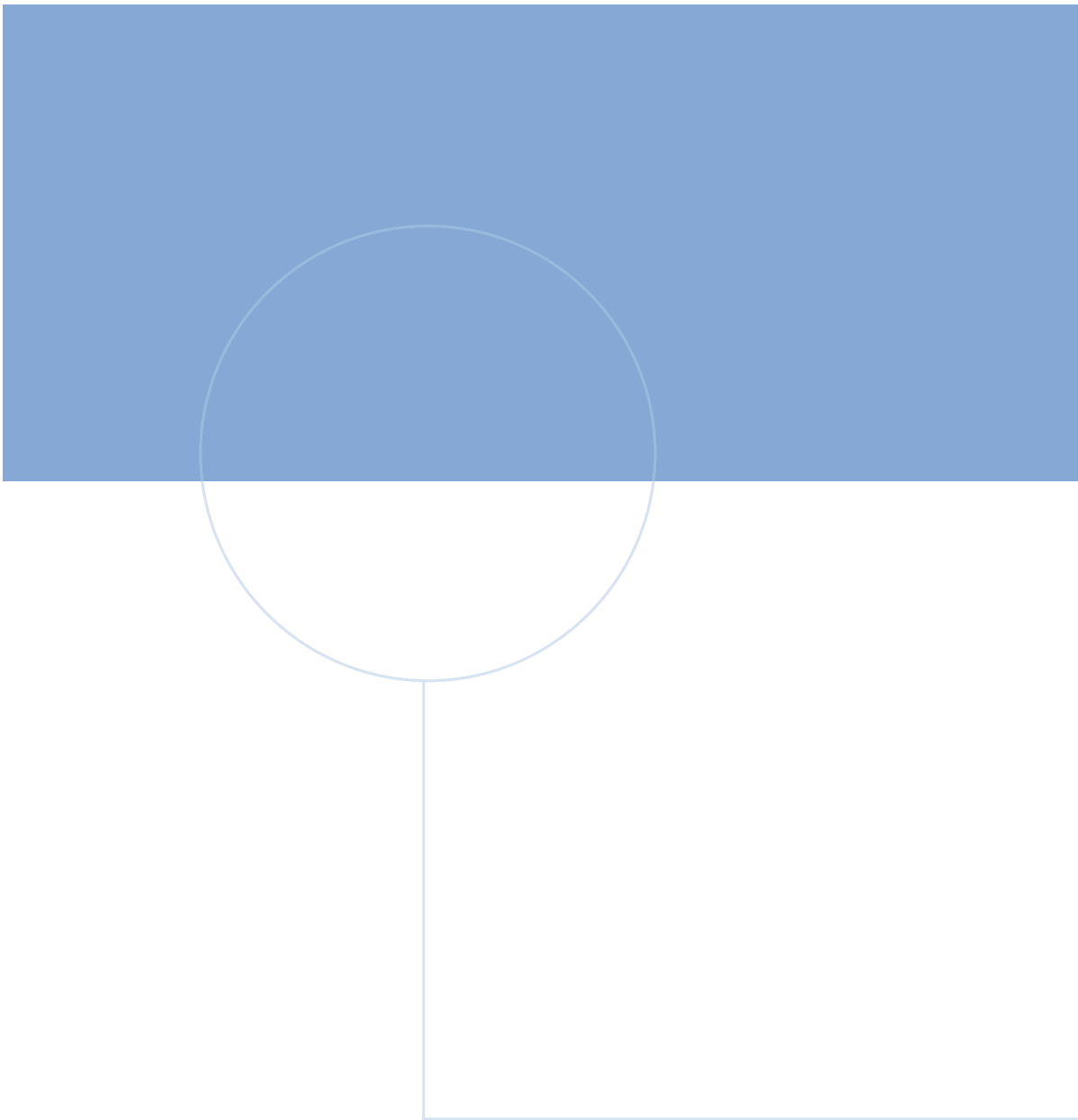

NTNU

Norwegian University of
Science and Technology